

Four-hour thunderstorm nowcasting using deep diffusion models of satellite

Author Information

Kuai Dai, Xutao Li*, Junying Fang, Yunming Ye*, Demin Yu, Di Xian, Danyu Qin, Jingsong Wang*

Affiliations

School of Computer Science and Technology, Harbin Institute of Technology, Shenzhen, China

Kuai Dai, Xutao Li, Yunming Ye, Demin Yu

Institute of Tropical and Marine Meteorology, China Meteorological Administration, Guangzhou, China

Junying Fang

National Satellite Meteorological Center, China Meteorological Administration, Beijing, China

Di Xian, Danyu Qin, Jingsong Wang

Corresponding authors

Correspondence to: Xutao Li, lixutao@hit.edu.cn; Yunming Ye, yeyunming@hit.edu.cn;

Jingsong Wang, wangjs@cma.gov.cn

Abstract

Convection (thunderstorm) develops rapidly within hours and is highly destructive, posing a significant challenge for nowcasting and resulting in substantial losses to nature and society. After the emergence of artificial intelligence (AI)-based methods, convection nowcasting has experienced rapid advancements, with its performance surpassing that of physics-based numerical weather prediction and other conventional approaches. However, the lead time and coverage of it still leave much to be desired and hardly meet the needs of disaster emergency response. Here, we propose deep diffusion models of satellite (DDMS) to establish an AI-based convection nowcasting system. On one hand, it employs diffusion processes to effectively simulate complicated spatiotemporal evolution patterns of convective clouds, significantly improving the forecast lead time. On the other hand, it utilizes geostationary satellite brightness temperature data, thereby achieving planetary-scale forecast coverage. During long-term tests and objective validation based on the FengYun-4A satellite, our system achieves, for the first time, effective convection nowcasting up to 4 hours, with broad coverage (about 20,000,000 km²), remarkable accuracy, and high resolution (15 minutes; 4 km). Its performance reaches a new height in convection nowcasting compared to the existing models. In terms of application, our system operates efficiently (forecasting 4 hours of convection in 8 minutes), and is highly transferable with the potential to collaborate with multiple satellites for global convection nowcasting. Furthermore, our results highlight the remarkable capabilities of diffusion models in convective clouds forecasting, as well as the significant value of geostationary satellite data when empowered by AI technologies.

Introduction

Severe convective weather often lead to sudden meteorological disasters like hailstorms, thunderstorms, strong winds, and tornadoes¹⁻³. These events have significant adverse effects on

various aspects of daily life and economic activities such as transportation, agriculture, energy production, and societal management⁴⁻⁶. As a conventional model for convective weather nowcasting and forecasting, the numerical weather prediction (NWP) solves the physical equations in the atmosphere to make predictions⁷. While the NWP has advantages in large-scale weather forecast from several hours to several days ahead, it tends to produce poor results in local nowcasting from the present to several hours ahead^{8,9}, because the convection in mesoscale or small scale plays a crucial role. One alternative type of method is the advection-based approaches such as STEPS¹⁰ or pySTEPS¹¹, which follow physical motion principles to extrapolate current states to the future. However, the advection-based approaches continue struggling to provide precise nowcasting outcomes due to two primary factors. On the one hand, the estimated advection tendency is unable to capture the intricateness of atmospheric motion and variation patterns, such as cloud formation and dissipation. On the other hand, these methods are limited in their ability to leverage extensive historical data for modeling nonlinear spatiotemporal dynamics, since they estimate the motion field based solely on the recent observations¹².

In recent years, artificial intelligence (AI) technologies¹³⁻¹⁵ largely promote the forward of weather nowcasting^{8,16}. With advanced neural network architectures¹⁷⁻²¹, the AI-based nowcasting models learn spatiotemporal evolution patterns from historical meteorological data in an end-to-end optimization manner. Once trained, such models can efficiently make predictions with given observations. As a pioneer AI-based method for precipitation nowcasting, ConvLSTM²² incorporates the convolution operation into LSTM¹⁷ to model spatiotemporal patterns of radar sequences and delivers promising results compared with traditional approaches. To alleviate the blurry issue of nowcasting results produced by ConvLSTM, DGMR⁸ introduces

generative adversarial networks (GANs)²³⁻²⁶ to improve the nowcasting results and achieves spatiotemporally consistent predictions with a lead time of 90 minutes. As a state-of-the-art precipitation nowcasting approach, NowcastNet¹⁶ designs a special evolution network to learn physical knowledge to guide prediction and achieves 3-hour extreme precipitation prediction. Despite the progress delivered by such existing AI-based nowcasting approaches, they still fall short due to their limited lead time, spatial scale, and accuracy, especially in heavy rainfall closely related to convection.

As satellite remote sensing technologies advance rapidly, the latest generation of stationary meteorological satellites now offers extensive atmospheric monitoring capabilities, enabling them to detect thunderstorm initiation earlier than radars²⁷⁻³². For convective monitoring utilizing the infrared brightness temperature band, they can achieve a high spatiotemporal resolution quite close to that of ground-based radars. Furthermore, convection nowcasting with stationary satellite has gained widespread adoption in meteorological departments globally³³⁻³⁵. Compared to nowcasting convective activities based on ground-based radar data (whether from single stations or networked), a prominent advantage of nowcasting convection using brightness temperatures from geostationary satellites is the ability to monitor large areas at a planetary scale, including continuous 24-hour coverage of remote regions and oceans where radar installations do not exist. Recent studies^{32,36} introduce AI techniques to convection nowcasting with satellite data and achieve promising results. However, they provide accurate convection nowcasting results only in a short period (20 minutes – 2 hours). The essential reason is the lack of stable and reliable AI architectures designed to model the spatiotemporal evolution patterns of convective clouds, especially in the reasonable simulation of stochastic and uncertain motion patterns in the temporal evolution process of convective clouds. Inspired by the natural advantages of diffusion

models in modeling stochastic processes³⁷, we argue that the stochastic motion tendency of convective clouds can be regarded as a physical diffusion process, which can be effectively modeled with forward and backward procedures of diffusion models^{38,39}.

Based on the insights above, we propose deep diffusion models of satellite (DDMS) to establish a convective nowcasting system utilizing satellite brightness temperature data, and conduct long-term tests and objective validation based on the FengYun-4A satellite. This forecasting system achieves, for the first time, effective convection nowcasting up to 4 hours, and features key forecasting capabilities such as broad coverage (about 20,000,000 km²), high accuracy, and high spatiotemporal resolution (15 minutes; 4 km). Its performance reaches a new height in convection nowcasting compared to both the existing state-of-the-art AI models and the most advanced traditional models. Moreover, the forecasting system is highly transferable, with relevant methodologies and algorithms that can be easily transferred across different satellite platforms. It operates efficiently, forecasting 16 time points within 4 hours in just 8 minutes, possessing significant operational forecasting application advantages.

High-Resolution Convection Nowcasting System

We develop a high-resolution convection nowcasting system with deep learning techniques. Specifically, we formulate the convection nowcasting task as two stages, namely, satellite nowcasting and convection detection. For the satellite nowcasting, we propose the DDMS to model spatiotemporal patterns of convective clouds to predict the next 4-hour satellite sequences. For the convection detection, we adopt a combined manner of deep learning and expert knowledge to achieve the convective clouds recognition. In this article, we utilize FengYun-4A satellite data⁴⁰ from 2018 to 2021 year as training data and employ 2022 and 2023 data as the

test data. The designed DDMS is trained on a GPU server with eight RTX A6000 (48GB memory) and takes two million training batches to coverage (about 30 days).

As shown in **Fig. 1**, the DDMS convection nowcasting system consists of a data process module, a satellite nowcasting module, and a convection detection module. First, in the data process module, collected FengYun-4A satellite images (AGRI-L1 RGEC and DISK data, 4km, 10.8 μ m-band) are first temporally sampled into sequences with a 15-minute interval, and then spatially cropped into 256×256 -size parts to reduce the GPU memory demand of satellite nowcasting module in the training phase. Second, the designed DDMS model is trained to predict the next 4-hour satellite sequences with historical 2-hour ones as input. Since our model is a fully convolutional network, once trained, it can be tested with arbitrary size sequences such as $1,280 \times 730$ -size (about 20,000,000 km² coverage). Third, the convection detection module accounts for automatically recognizing the convective clouds in the predicted satellite sequences. To achieve this, we manually label a convective cloud dataset based on FengYun-4A with the guidance of experts in the National Satellite Meteorological Center and train an UNet to detect the convective clouds.

Through the three modules, we build a high-resolution convection nowcasting system. It significantly surpasses the state-of-the-art traditional nowcasting approach pySTEPS and the AI-based nowcasting method NowcastNet in terms of quantitative evaluation. Besides, in the severe convective weather events evaluation, our method accurately predicts the locations and intensity of convective clouds while the other baseline methods fail to do this.

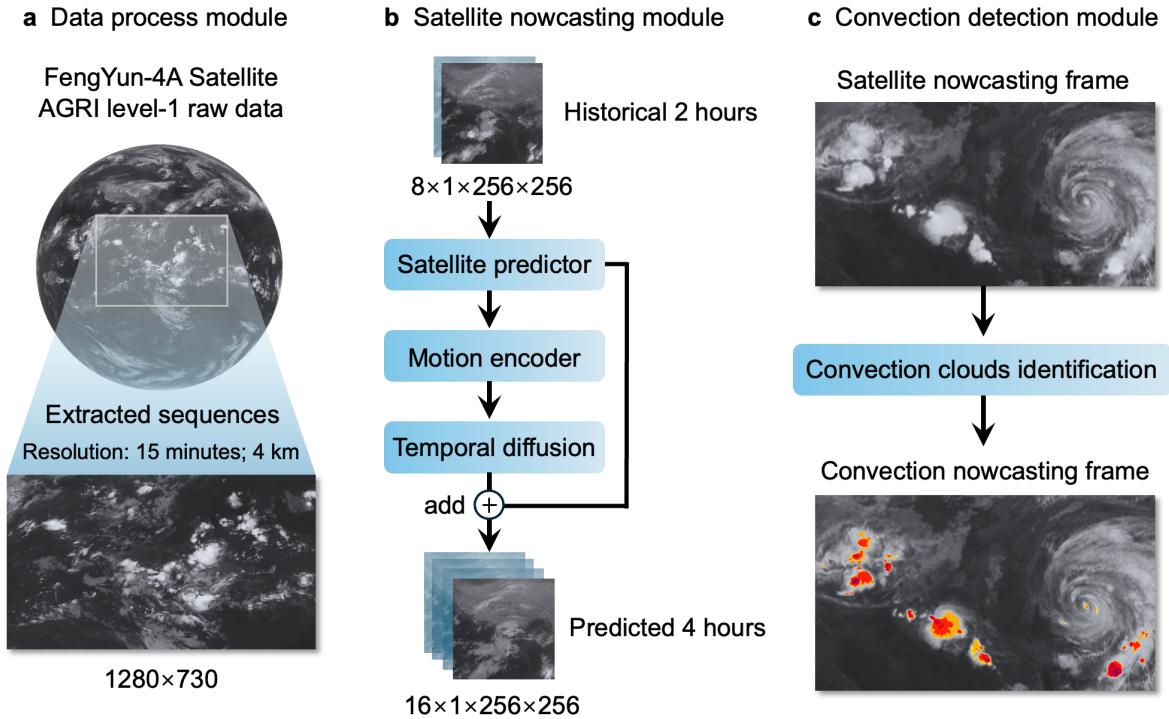


Fig. 1 Framework of DDMS convection nowcasting system. **a**, Data process module, collected FengYun-4A AGRI-L1-RGEC and DISK data are processed into regular satellite sequences through spatial cropping and temporal sampling operations. **b**, Satellite nowcasting module, predicts the next 4-hour satellite data based on the historical 2-hour satellite data. **c**, Convection detection module, identifies the convective clouds in the predicted satellite sequences.

Results

Evaluation Settings.

We validate the nowcasting ability of the proposed DDMS against the state-of-the-art traditional and AI-based prediction methods. We employ pySTEPS¹¹, an advection-based nowcasting method, as the baseline of traditional methods, which has been widely used in meteorological centers worldwide^{10,41}. We select NowcastNet¹⁶ as another baseline of deep learning methods, which delivers state-of-the-art performance for 3-hour radar nowcasting. In this work, we utilize FengYun-4A satellite $10.8\mu\text{m}$ -band observations in 2018-2021 to train the above models, and employ spring and summer samples (May to August) in 2022-2023 to

validate the nowcasting performance. During these months, the motions of convective clouds are most fierce, and the clouds' growth and decay are common in East Asia, accompanied by abrupt meteorological disasters.

Convection Nowcasting Results.

Quantitative Evaluation.

Fig. 2 shows the quantitative convection nowcasting results of DDMS, NowcastNet, and pySTEPS. The critical success index (CSI) is a key evaluation metric, which measures the nowcasting accuracy in terms of locations of convective clouds. Another key evaluation metric, mean absolute error (MAE), can simultaneously reflecting the accuracy of predicted convection with respect to locations and intensity. Overall, the higher CSI score, the better, while the lower MAE score, the better. Specifically, we conduct experiments using FengYun-4A data from 2022 and 2023 to validate the prediction stability of the nowcasting methods across different years.

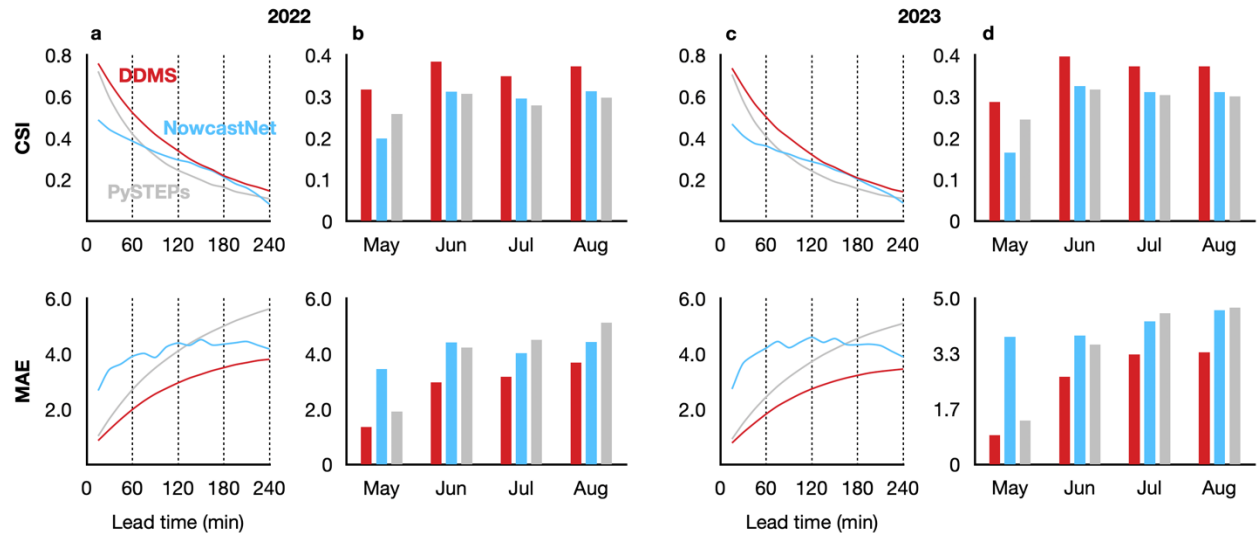


Fig. 2 Quantitative evaluation of DDMS. Curves of the critical success index (CSI) and mean absolute error (MAE) with nowcasting lead time averaged from May to August in 2022 (a) and 2023 (c). Histograms of the CSI and MAE respectively for 2022 (b) and 2023 (d) May, June, July, and August. Red (blue, grey) curves and bars indicate DDMS (NowcastNet, pySTEPS).

Specifically, when compared to the traditional method pySTEPS, DDMS shows the superiority both in terms of forecasting location (CSI) and intensity (MAE) of convective clouds (**Fig. 2a, c**). Moreover, the superiority becomes more obvious as the lead time goes by, especially in terms of the intensity. When compared to the AI-based method NowcastNet, DDMS consistently outperforms it during the 4-hour convection nowcasting (CSI). Notably, NowcastNet delivers competitive results against DDMS during a short period (from 150 minutes to 180 minutes), while it performs much worse than DDMS during other periods. As for intensity (MAE) evaluation, DDMS demonstrates significant superiority during the 4 hours. The observations indicate that DDMS has advantages in modeling 4-hour temporal dynamics of satellite sequences and can simultaneously accurately forecast the location and intensity of convective clouds compared to state-of-the-art models.

We also evaluate convection nowcasting results of DDMS in May, Jun, July, and August (**Fig. 2b, d**). Intuitively, DDMS delivers the best performance in all months in terms of location (CSI) and intensity (MAE). Note that the overall 4-hour forecast performance of NowcastNet for the location and intensity of convection is similar to that of pySTEPS, and it may even perform worse than pySTEPS in May and June. In contrast, DDMS consistently demonstrates superior performance across all months. Specifically, in the 2022 year, the proposed DDMS outperforms pySTEPS (the second best) by 22.83% on CSI score in May, outperforms NowcastNet (the second best) by 23.22% on CSI score in June, by 17.93% on CSI score in July, by 19.10% on CSI score in August, respectively. In the 2023 year, the proposed DDMS outperforms pySTEPS by 17.13% on CSI score in May, outperforms NowcastNet by 22.04% on CSI score in June, by 20.13% on CSI score in July, by 20.05% on CSI score in August, respectively. As for the MAE evaluation in the 2022 year, DDMS outperforms pySTEPS by 28.53% on MAE score in May, by

29.72% on MAE score in June, respectively, outperforms NowcastNet by 21.11% on MAE score in July, by 17.03% on MAE score in August, respectively. In the 2023 year, the proposed DDMS outperforms pySTEPS by 32.89% on MAE score in May, by 26.92% on MAE score in June, respectively, outperforms NowcastNet by 23.20% on MAE score in July, by 27.25% on MAE score in August, respectively. The observations demonstrate that DDMS can better recognize and model spatiotemporal patterns of convective clouds across different months while the state-of-the-art nowcasting baselines fail to do this.

Case Evaluation.

To visually evaluate the nowcasting ability of DDMS, we report two nowcasting results of typical severe convection events in **Fig. 3** and **Fig. 4**. The pySTEPS preserves sharp appearance details but fails to accurately predict the complicated motion tendency of clouds, which are far away from observations. The advection-based physical equations are hard to characterize the non-stationary motion patterns of clouds such as rotation, dissipation, and accumulation. Compared with pySTEPS, NowcastNet makes more accurate predictions in 2-hour nowcasting, where the predicted convective clouds are more accurate. However, NowcastNet delivers much blurrier nowcasting results than pySTEPS. Both methods' prediction ability degrades dramatically, and can hardly deliver a practical prediction at 4 hours. By contrast, DDMS makes sharp predictions and delivers much more accurate 4-hour nowcasting results in terms of the location, size, and intensity of convective clouds. More convection nowcasting samples are provided in the supplementary file.

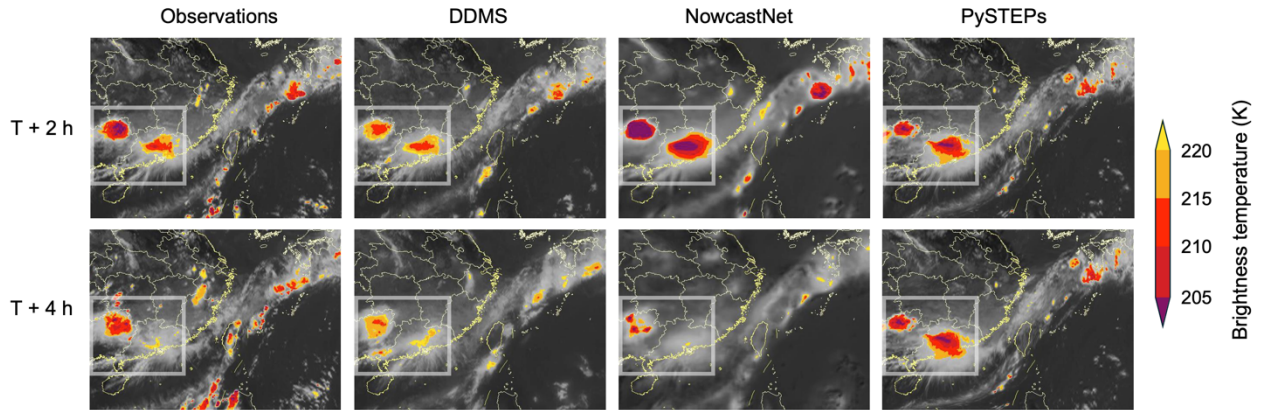


Fig. 3 Case evaluation of a severe convection event with extreme rainstorm starting on 16 June 2022 in South China. This convection event is also accompanied by floods warning of the Pearl River. The color denotes the predicted brightness temperature (K) of convective clouds. The locations of the extreme event are marked with white boxes. The samples are cropped to highlight local details. The state-of-the-art AI-based nowcasting baseline method NowcastNet significantly underestimates the motion tendency of convective clouds 4 hours later. The traditional baseline approach pySTEPS fails to model the growth and death of convective clouds and significantly overestimates the motion tendency of convective clouds. The two methods fail to deliver satisfactory 4-hour convection nowcasting, while our proposed DDMS produces much more accurate nowcasting results.

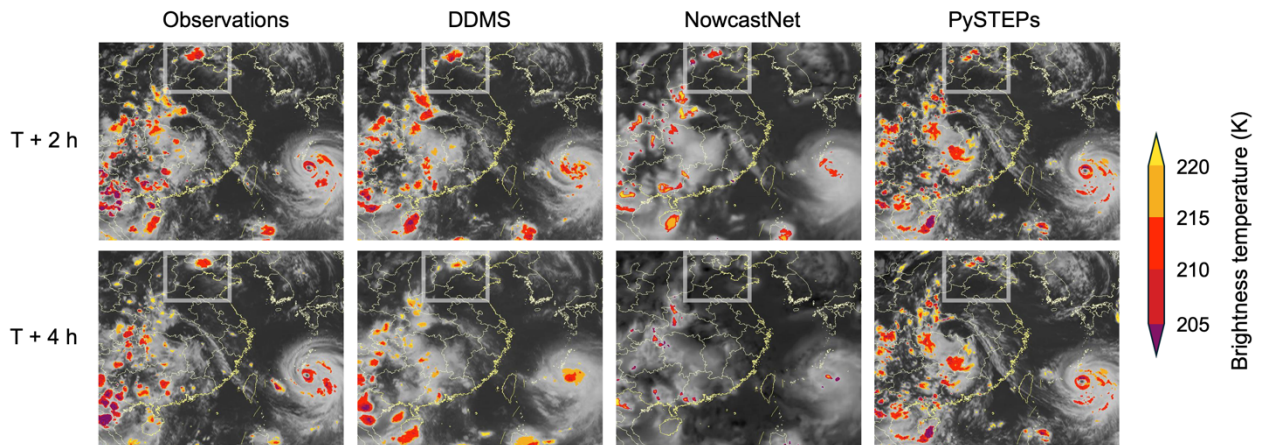


Fig. 4 Case evaluation of a severe convection event with extreme rainstorm starting on 29 July 2023 in Beijing-Tianjin-Hebei region of China. This convection event is affected by the typhoon Dusui (in the rightdown corner). The color denotes the predicted brightness temperature of convective clouds. The locations of the extreme event are marked with white boxes. The samples are cropped to highlight local details. Again, DDMS delivers accurate nowcasting results while the state-of-the-art baselines fail to do this.

Discussion

In this article, we propose DDMS and build a high-resolution convection nowcasting system of satellite data. Our model is trained on 2018-2021 FengYun-4A satellite data and tested on 2022-2023 data. Compared with state-of-the-art nowcasting baseline approaches, DDMS consistently delivers the best and skilfull 4-hour convection nowcasting results in terms of quantitative and case evaluation. Note that our nowcasting system can produce 4-hour convection nowcasting with broad coverage (about 20,000,000 km²) in 8 minutes, which fits the nowcasting requirements in practical scenarios.

Convection nowcasting can be further improved from some aspects. In terms of methodology, more efficient AI techniques can be explored to deliver more accurate and higher spatio-temporal resolution convection nowcasting. Besides, from the perspective of data, fusing multi-source such as satellite and radar data can promote the accuracy and interpretability of AI-based methods for convection nowcasting. Also, DDMS's training cost is very large due to the diffusion architecture, and it is important to explore more efficient diffusion models^{42,43}. At last, explicitly incorporating the conventional physical knowledge as constraint for AI-based methods is a promising direction. We hope our work can inspire more researchers to investigate convection nowcasting with meteorological satellite data.

References

1. Dotzek, N., Groenemeijer, P., Feuerstein, B., & Holzer, A. M. Overview of ESSL's severe convective storms research using the European Severe Weather Database ESWD. *Atmospheric research*, 93 (1-3), 575-586 (2009).
2. Melhauser, C., & Zhang, F. Practical and intrinsic predictability of severe and convective weather at the mesoscales. *Journal of the Atmospheric Sciences*, 69 (11), 3350-3371 (2012).

3. Tippet, M. K., Allen, J. T., Gensini, V. A., & Brooks, H. E. Climate and hazardous convective weather. *Current Climate Change Reports*, 1, 60-73 (2015).
4. Castle, J., Hendry, D., & Kitov, O. *Forecasting and nowcasting macroeconomic variables: A methodological overview*. (Press, Eurostat, 2017).
5. Wilson, J. W., Feng, Y., Chen, M., & Roberts, R. D. Nowcasting challenges during the Beijing Olympics: Successes, failures, and implications for future nowcasting systems. *Weather and Forecasting*, 25 (6), 1691-1714 (2010).
6. Han, L., Sun, J., Zhang, W., Xiu, Y., Feng, H., & Lin, Y. A machine learning nowcasting method based on real-time reanalysis data. *Journal of Geophysical Research: Atmospheres*, 122 (7), 4038-4051 (2017).
7. Toth, Z., & Kalnay, E. Ensemble forecasting at NCEP and the breeding method. *Monthly Weather Review*, 125 (12), 3297-3319 (1997).
8. Ravuri, S., Lenc, K., Willson, M., Kangin, D., Lam, R., Mirowski, P., ... & Mohamed, S. Skilful precipitation nowcasting using deep generative models of radar. *Nature*, 597 (7878), 672-677 (2021).
9. Pierce, C., Seed, A., Ballard, S., Simonin, D. & Li, Z. Doppler radar observations: Weather radar, wind profiler, ionospheric radar, and other advanced applications. (eds Bech, J. & Chau, J. L.) 97–142 (IntechOpen, 2012).
10. Bowler, N. E., Pierce, C. E., & Seed, A. W. STEPS: A probabilistic precipitation forecasting scheme which merges an extrapolation nowcast with downscaled NWP. *Quarterly Journal of the Royal Meteorological Society*, 132 (620), 2127-2155. (2006).

11. Pulkkinen, S., Nerini, D., Pérez Hortal, A. A., Velasco-Forero, C., Seed, A., Germann, U., & Foresti, L. Pysteps: An open-source Python library for probabilistic precipitation nowcasting (v1. 0). *Geoscientific Model Development*, 12 (10), 4185-4219 (2019).
12. Dai, K., Li, X., Ye, Y., Feng, S., Qin, D., & Ye, R. MSTCGAN: Multiscale time conditional generative adversarial network for long-term satellite image sequence prediction. *IEEE Transactions on Geoscience and Remote Sensing*, 60, 1-16. (2022).
13. Shi, X., Chen, Z., Wang, H., Yeung, D. Y., Wong, W. K., & Woo, W. C. Convolutional LSTM network: A machine learning approach for precipitation nowcasting. *Proceedings of the Advances in neural information processing systems*, 28 (2015).
14. Ballas, N., Yao, L., Pal, C., & Courville, A. Delving deeper into convolutional networks for learning video representations. *Proceedings of the International Conference on Learning Representations* (2015).
15. Wang, Y., Wu, H., Zhang, J., Gao, Z., Wang, J., Philip, S. Y., & Long, M. Predrnn: A recurrent neural network for spatiotemporal predictive learning. *IEEE Transactions on Pattern Analysis and Machine Intelligence*, 45 (2), 2208-2225 (2022).
16. Zhang, Y., Long, M., Chen, K., Xing, L., Jin, R., Jordan, M. I., & Wang, J. Skilful nowcasting of extreme precipitation with NowcastNet. *Nature*, 619 (7970), 526-532 (2023).
17. Hochreiter, S., & Schmidhuber, J. Long short-term memory. *Neural computation*, 9 (8), 1735-1780 (1997).
18. Chung, J., Gulcehre, C., Cho, K., & Bengio, Y. Empirical evaluation of gated recurrent neural networks on sequence modeling. *Proceedings of the Advances in neural information processing systems workshop* (2014).

19. Krizhevsky, A., Sutskever, I., & Hinton, G. E. Imagenet classification with deep convolutional neural networks. Proceedings of the Advances in neural information processing systems, 25 (2012).
20. Vaswani, A., Shazeer, N., Parmar, N., Uszkoreit, J., Jones, L., Gomez, A. N., Kaiser, Ł. & Polosukhin, I. Attention is all you need. Proceedings of the Advances in neural information processing systems, 30 (2017).
21. Bi, K., Xie, L., Zhang, H., Chen, X., Gu, X., & Tian, Q. Accurate medium-range global weather forecasting with 3D neural networks. Nature, 619(7970), 533-538 (2023).
22. Shi, X., Chen, Z., Wang, H., Yeung, D. Y., Wong, W. K., & Woo, W. C. Convolutional LSTM network: A machine learning approach for precipitation nowcasting. Proceedings of the Advances in neural information processing systems, 28 (2015).
23. Goodfellow, I., Pouget-Abadie, J., Mirza, M., Xu, B., Warde-Farley, D., Ozair, S., Courville, A. & Bengio, Y. Generative adversarial nets. Proceedings of the Advances in neural information processing systems, 27 (2014).
24. Radford, A., Metz, L., & Chintala, S. Unsupervised representation learning with deep convolutional generative adversarial networks. Proceedings of the International Conference on Learning Representations (2015).
25. Arjovsky, M., Chintala, S., & Bottou, L. Wasserstein generative adversarial networks. Proceedings of the International Conference on Machine Learning, 214-223 (2017).
26. Miyato, T., Kataoka, T., Koyama, M., & Yoshida, Y. Spectral Normalization for Generative Adversarial Networks. Proceedings of the International Conference on Learning Representations (2018).

27. Sieglaff, J. M., Crounce, L. M., Feltz, W. F., Bedka, K. M., Pavolonis, M. J., & Heidinger, A. K. Nowcasting convective storm initiation using satellite-based box-averaged cloud-top cooling and cloud-type trends. *Journal of applied meteorology and climatology*, 50 (1), 110-126 (2011).
28. Kober, K., & Tafferner, A. Tracking and nowcasting of convective cells using remote sensing data from radar and satellite. *Meteorologische Zeitschrift*, 1, 75-84 (2009).
29. Bedka, K., Brunner, J., Dworak, R., Feltz, W., Otkin, J., & Greenwald, T. Objective satellite-based detection of overshooting tops using infrared window channel brightness temperature gradients. *Journal of applied meteorology and climatology*, 49 (2), 181-202 (2010).
30. Ai, Y., Li, J., Shi, W., Schmit, T. J., Cao, C., & Li, W. Deep convective cloud characterizations from both broadband imager and hyperspectral infrared sounder measurements. *Journal of Geophysical Research: Atmospheres*, 122 (3), 1700-1712 (2017).
31. Takahashi, H., & Luo, Z. J. Characterizing tropical overshooting deep convection from joint analysis of CloudSat and geostationary satellite observations. *Journal of Geophysical Research: Atmospheres*, 119 (1), 112-121 (2014).
32. Lagerquist, R., Stewart, J. Q., Ebert-Uphoff, I., & Kumler, C. Using deep learning to nowcast the spatial coverage of convection from Himawari-8 satellite data. *Monthly Weather Review*, 149(12), 3897-3921 (2021).
33. Mecikalski, J. R., Rosenfeld, D., & Manzato, A. Evaluation of geostationary satellite observations and the development of a 1–2 h prediction model for future storm intensity. *Journal of Geophysical Research: Atmospheres*, 121(11), 6374-6392 (2016).

34. Walker, J. R., MacKenzie Jr, W. M., Mecikalski, J. R., & Jewett, C. P. An enhanced geostationary satellite-based convective initiation algorithm for 0–2-h nowcasting with object tracking. *Journal of Applied Meteorology and Climatology*, 51(11), 1931-1949 (2012).
35. Mecikalski, J. R., & Bedka, K. M. Forecasting convective initiation by monitoring the evolution of moving cumulus in daytime GOES imagery. *Monthly Weather Review*, 134(1), 49-78 (2006).
36. Lee, S., Han, H., Im, J., Jang, E., & Lee, M. I. Detection of deterministic and probabilistic convection initiation using Himawari-8 Advanced Himawari Imager data. *Atmospheric Measurement Techniques*, 10(5), 1859-1874 (2017).
37. Sohl-Dickstein, J., Weiss, E., Maheswaranathan, N., & Ganguli, S. Deep unsupervised learning using nonequilibrium thermodynamics. *Proceedings of the International Conference on Machine Learning* 2256-2265 (2015).
38. Ho, J., Jain, A., & Abbeel, P. Denoising diffusion probabilistic models. *Proceedings of the Advances in Neural Information Processing Systems*, 33, 6840-6851 (2020).
39. Song, J., Meng, C., & Ermon, S. Denoising diffusion implicit models. *Proceedings of the International Conference on Learning Representations* (2020).
40. Xian, D., Zhang, P., Gao, L., Sun, R., Zhang, H., & Jia, X. Fengyun meteorological satellite products for earth system science applications. *Advances in Atmospheric Sciences*, 38(8), 1267-1284 (2021).

41. Imhoff, R. O., Brauer, C. C., Overeem, A., Weerts, A. H., & Uijlenhoet, R. Spatial and temporal evaluation of radar rainfall nowcasting techniques on 1,533 events. *Water Resources Research*, 56 (8), e2019WR026723 (2020).
42. Rombach, R., Blattmann, A., Lorenz, D., Esser, P., & Ommer, B. High-resolution image synthesis with latent diffusion models. *Proceedings of the IEEE/CVF conference on computer vision and pattern recognition*, 10684-10695 (2022).
43. Blattmann, A., Rombach, R., Ling, H., Dockhorn, T., Kim, S. W., Fidler, S., & Kreis, K. Align your latents: High-resolution video synthesis with latent diffusion models. *Proceedings of the IEEE/CVF Conference on Computer Vision and Pattern Recognition*, 22563-22575 (2023).

Methods

Here we introduce the details of the data process module, satellite nowcasting module, and convection detection module in the high-resolution convection nowcasting systems, as well as the evaluation metrics and training settings.

Data Process Module.

In this article, we collect FengYun-4A meteorological satellite AGRI-L1 data, from 2018 to 2023 year. Data in 2018-2021 years are utilized for training satellite nowcasting module while the remainder part is for convection nowcasting evaluation. With a multichannel visible infrared scanning imager, FengYun-4A can produce 14-waveband satellite images, where different wavebands aim at capturing different meteorological elements such as water vapor and temperature. To achieve convection nowcasting, we select the 12th channel (10.8 μ m-band, long-wave infrared) images with 4km spatial resolution, which is suitable for observing the convective

clouds in the atmosphere. The FengYun-4A satellite scans the China area (REGC) and the entire observation area (DISK) with an interval of 4-6 minutes and 15 minutes, respectively. First, we extract 24-frame sequences with an interval of 15 minutes, where each frame is $1,280 \times 730$ -size. Second, to save the training memory demand, we crop 256×256 -size parts of each frame. In this manner, we obtain 441,895 sequences for training the satellite nowcasting module and 4355 sequences for validation, respectively.

Satellite Nowcasting Module.

As shown in **Extended Data Fig. 1**, the module consists of three parts, namely, a satellite predictor P , a motion encoder M , and a temporal diffusion part D . First, the satellite predictor accounts for producing the predicted satellite sequence $\hat{Y} = \{\hat{X}_{l+1}, \hat{X}_{l+2}, \dots, \hat{X}_{l+k}\} \in \mathbb{R}^{k \times m \times n}$, with given the past frames $X = \{X_1, X_2, \dots, X_l\} \in \mathbb{R}^{l \times m \times n}$. m and n denote the width and length of each satellite image, respectively. Second, the temporal diffusion part is specially designed to model the temporal evolution dynamics of divergence between the predicted sequence \hat{Y} and observation sequence $Y = \{X_{l+1}, X_{l+2}, \dots, X_{l+k}\}$. Third, the motion encoder is designed to capture the long-term motion tendency of the predicted sequence \hat{Y} , to guide the denoising process of the temporal diffusion part. By combining the predicted sequence by satellite predictor P and the reconstructed difference sequence by temporal diffusion D , we obtain the final prediction sequence $\hat{Y}_{final} = P(x) + D(Y - \hat{Y})$. Next, we introduce details of the three parts and the training loss of the satellite nowcasting module.

Satellite Predictor. Overall, the satellite predictor follows a classic RNN architecture ConvGRU¹⁴, which is a simple yet effective spatiotemporal prediction baseline. Compared with

ConvLSTM, it adopts fewer inner memory units to model temporal evolution dynamics of sequences, whose key formulae are defined as follows:

$$\begin{aligned}
z_t &= \sigma(W_{xz} * \mathcal{X}_t + W_{hz} * \mathcal{H}_{t-1} + b_z), \\
r_t &= \sigma(W_{xr} * \mathcal{X}_t + W_{hr} * \mathcal{H}_{t-1} + b_r), \\
\tilde{\mathcal{H}}_t &= \tanh(W_{xh} * \mathcal{X}_t + W_{hh} * (r_t \circ \mathcal{H}_{t-1}) + b_h), \\
\mathcal{H}_t &= (1 - z_t) \circ \mathcal{H}_{t-1} + z_t \circ \tilde{\mathcal{H}}_t.
\end{aligned} \tag{1}$$

The z_t and r_t denote the update gate and reset gate, respectively. The $\tilde{\mathcal{H}}_t$ and \mathcal{H}_t represent the candidate hidden state and final hidden state, respectively. The $*$ is the convolution operation, the matrixes like W_{xz} and W_{hz} are corresponding weights, and terms like b_z , b_r , and b_h are biases. σ and \tanh are activation functions, and the symbol \circ denotes the Hadamard multiplication.

Based on the classic ConvGRU backbone, the satellite predictor introduces the deep residual mechanism and skip connection manner to enhance spatiotemporal modeling ability. Specifically, it contains an encoder part and a decoder part. In the encoder, three ResNet-GRU-Conv block layers and one ResNet-GRU block layer are utilized to encode multi-level spatiotemporal dynamics of satellite sequences. In the decoder, three ResNet-DeConv block layers and one convolutional layer with a kernel size of 1 are employed to produce predicted frames by decoding the multi-level spatiotemporal features. Notably, in each time step, different level hidden states generated by the GRU units in the encoder are passed to the decoder with a skip connection manner, which can better preserve spatial details. In an autoregressive manner, the satellite predictor produces the k-length predicted sequence.

Motion Encoder. The motion encoder adopts the previous four layers of a satellite predictor to encode the predicted sequence to obtain different level motion patterns at each time step, which are utilized to guide the denoising process of the temporal diffusion part. In particular, the

motion encoder does not share parameters with the satellite predictor, and is removed the skip connection operations. The encoding procedure is formally defined as follows:

$$\text{Motions}^i = M(\hat{Y}_i), \quad (2)$$

$$\text{Motions}^i = \{ \text{Motion}_1^i, \text{Motion}_2^i, \text{Motion}_3^i, \text{Motion}_4^i \}. \quad (3)$$

The Motion_1^i , Motion_2^i , Motion_3^i , and Motion_4^i denote different level motion patterns at the i -th time step.

Temporal Diffusion. With the guidance of the motion encoder, the temporal diffusion part is proposed to model the temporal evolution of the difference satellite sequence. To train the diffusion network, we adopt a training paradigm provided by DDPM³⁸, which treats the diffusion process as a first-order Markov-chain procedure. Specifically, in the forward process, Gaussian noise is gradually added to destroy the original data x_0 , then we obtain T different states $\{x_1, x_2, \dots, x_T\}$, which is formally defined as follows:

$$q(x_{1:T} | x_0) = \prod_{t=1}^T q(x_t | x_{t-1}), \quad (4)$$

$$q(x_t | x_{t-1}) = \mathcal{N}(x_t | \sqrt{\alpha_t}x_{t-1}, (1 - \alpha_t)\mathbf{I}). \quad (5)$$

$1 - \alpha_t$ is the predefined covariance hyperparameter at the t -th time step. $\alpha_t \in (0,1), t \in \{1,2, \dots, T\}$, and $\alpha_1 > \alpha_2 > \dots > \alpha_T$. Through formulae (4) and (5), t -th state x_t can be obtained in one step as follows:

$$q(x_t | x_0) = \int q(x_{1:t} | x_0) dx_{1:(t-1)} = \mathcal{N}(x_t | \sqrt{\bar{\alpha}_t}x_0, (1 - \bar{\alpha}_t)\mathbf{I}), \quad (6)$$

where $\bar{\alpha}_t = \alpha_1 \alpha_2 \dots \alpha_t$. When $t \rightarrow \infty$, then $\bar{\alpha}_t \rightarrow 0$, and we can get that $x_t \rightarrow \mathcal{N}(0, \mathbf{I})$.

In the reverse process, we aim to recover the original data x_0 from the Gaussian noise x_T . Formally, the denoising process is defined as follows:

$$p(x_0) = \int p(x_{0:T}) dx_{1:T}, \quad (7)$$

$$p(x_{0:T}) = p(x_T) \prod_{t=1}^T p(x_{t-1} | x_t), \quad (8)$$

$$p(x_{t-1} | x_t) = \mathcal{N}(x_{t-1} | \mu(x_t, t), \sigma_t \mathbf{I}). \quad (9)$$

The $p(x_T) = \mathcal{N}(0, \mathbf{I})$ is known, and the σ_t is fixed and computed by $\bar{\alpha}_t$. The mean value $\mu(x_t, t)$ needs to be learned and depends on Gaussian noise. For this, DDPM adopts a UNet model f_θ to predict the noise ϵ . In this work, we employ the multi-level motion patterns at the i -th time step Motions^i , as a condition to help the UNet to predict the noise. Hence, the training loss function of the denoising process is as follows:

$$L(\theta) = \mathbb{E}_{\mathbf{x}_0, t, \epsilon} \|\epsilon - f_\theta(\mathbf{x}_t, t, \text{Motions}^i)\|^2, \quad (10)$$

$$x_t = \sqrt{\bar{\alpha}_t} x_0 + \sqrt{1 - \bar{\alpha}_t} \epsilon. \quad (11)$$

Training Loss. We employ a predicted loss, namely, mean absolute error loss, to train the satellite predictor. We use a diffusion loss to train the temporal diffusion part. By combining the two loss terms, we obtain the training loss of the satellite nowcasting module as follows:

$$L(\hat{Y}, Y) = \sum_{i=1}^k (|Y_i - \hat{Y}_i| + \lambda * \text{Diff}(Y_i - \hat{Y}_i)). \quad (12)$$

The coefficient λ is utilized to balance the two loss terms. $\text{Diff}(\cdot)$ is implemented by optimizing formulae (10) and (11), where the initial state $x_0 = Y_i - \hat{Y}_i$.

Convection Detection Module.

Traditional convection detection on satellite images usually relies on a specific threshold value to judge convective clouds, in which the threshold value is obtained according to meteorologists' experiential judgment. As for the 10.8 μ m-band FengYun-4A data, the grids are regarded as convective clouds, whose brightness temperature of each grid is lower than 210K (provided by the National Satellite Meteorological Center). The threshold detection approach is simple but not very robust, and its accuracy is also a main concern. To automatically detect the convective clouds in the predicted satellite sequence, our team and experts in the National Satellite Meteorological Center manually label a convection dataset. Specifically, we label the convective clouds by combining four principles, namely, the basic characteristics of convective clouds summarized by experts, satellite images in visible channels, the brightness temperature of satellite data, and corresponding radar maps. The detailed label principles are described in the appendix. Then we utilize the convection dataset to train a detection model (2D-UNet⁴⁴). Finally, the convection nowcasting results are obtained by segmenting each frame of the predicted satellite sequence produced by the satellite nowcasting module with the pretrained detection model.

Evaluation Metrics.

For quantitative evaluation, we utilize two commonly used metrics in weather nowcasting including critical success index (CSI) and mean absolute error (MAE) to evaluate the convection nowcasting results. Both the CSI and MAE scores measure nowcasting accuracy, the CSI emphasizes location while MAE concentrates on intensity. The metrics are formally defined as follows:

$$CSI = \frac{TP}{TP + FN + FP}, \quad (13)$$

$$MAE = |\hat{Y}_{final} \odot \hat{C} - Y \odot C|. \quad (14)$$

With the convection detection module, the predicted satellite sequences \hat{Y}_{final} are binarized to the convection sequences \hat{C} . Then we can obtain the true positives (TP, prediction = 1, target = 1), false positives (FP, prediction = 1, target = 0), and false negatives (FN, prediction = 0, target = 1), to calculate the CSI score. The Y and C represent the ground-truth satellite sequences and corresponding detection results, respectively. The \odot denotes the Hadamard product, and the MAE is obtained by computing the error between the predicted convection results $\hat{Y}_{final} \odot \hat{C}$ and convection observations $Y \odot C$.

Implementation Details.

Our model DDMS is trained on a GPU server with a CPU of Intel(R) Xeon(R) Gold 6130 CPU @ 2.10GHz, 256G memory, and 8 RTX A6000 cards (48G memory). We utilize the Adam optimizer⁴⁵ to train the model, and use the exponential moving average (EMA) strategy⁴⁶ with a decay weight of 0.99 to update the parameters. The batch size and learning rate are set to 8 and 5e-5, respectively. The weight λ in the combined training loss is 10. The dimensions of hidden states in the four-layer GRU are set to 64, 128, 192, and 256, respectively. As for the diffusion part, the forwarding step is set to 1000, while the denoising step is set to 200 with a DDIM³⁹ sampling manner. The details and analysis of our model are shown in the supplementary material.

Data Availability

The FengYun-4A AGRI-4km-L1 satellite data (about 18T) can be free downloaded from the website [<http://data.nsmc.org.cn/portalsite/default.aspx>]. The satellite data comprises two types:

DISK and REGC. DISK data covers the entire disk region, while REGC data specifically focuses on the China area. We combine these two types of data and extract sequences of 24 frames at 15-minute intervals. In addition, the test satellite data and corresponding labeled convection data will be provided soon.

Code Availability

In this work, we utilize pytorch [<https://pytorch.org/>], a widely used deep learning framework, to train our model. We use Python [<https://www.python.org/>] to complete the data process and results evaluation. In particular, we use the h5py to load the FengYun-4A HDF files and employ opencv-python to read and save the processed satellite images. The quantitative metrics such as CSI and MAE are calculated on the Python library Numpy. Besides, we utilize the pySTEPS [<https://pysteps.github.io/>] and NowcastNet [<https://codeocean.com/capsule/3935105/tree/v1>] as baselines to achieve convection nowcasting. The prediction samples of DDMS over different months are provided in [<https://github.com/bigfeetsmalltone/DDMS>]. The source codes of DDMS and its pretrained weight will be provided soon. The source codes of the convection detection model are available from the corresponding author upon request.

44. Ronneberger, O., Fischer, P., & Brox, T. U-net: Convolutional networks for biomedical image segmentation. Proceedings of the Medical Image Computing and Computer-Assisted Intervention, Part III 18, 234-241 (2015).
45. Kingma, D. P., & Ba, J. Adam: A method for stochastic optimization. Proceedings of the International Conference on Learning Representations (2015).

46. Tarvainen, A., & Valpola, H. Mean teachers are better role models: Weight-averaged consistency targets improve semi-supervised deep learning results. Proceedings of the Advances in Neural Information Processing Systems, 30, 1195-1204 (2017).

Acknowledgements

This work was supported by NSFC under Grants 62376072, 62272130, and Shenzhen Science and Technology Program under Grant JCYJ20200109113014456 and Grant KCXFZ20211020163403005, Guangdong Basic and Applied Basic Research Foundation (2023A1515110811, J.F.), and FengYun Application Pioneering Project under Grant FY-APP-ZX-2022.0220.

Author contributions

Kuai Dai, Xutao Li, Yunming Ye, and Jingsong Wang conceived and designed the work. Kuai Dai, Xutao Li, Yunming Ye, and Demin Yu discussed details of the designed method and experimental results. Kuai Dai achieved the coding for the data process, model training, and results evaluation and completed manuscript writing. Junying Fang conducted investigation, visualization, and revision of the manuscript. Di Xian, Danyu Qin, and Jingsong Wang constructed the convection data and participated in data processing and case analysis. All the authors contributed edits.

Competing interests

The authors declare no competing interests.

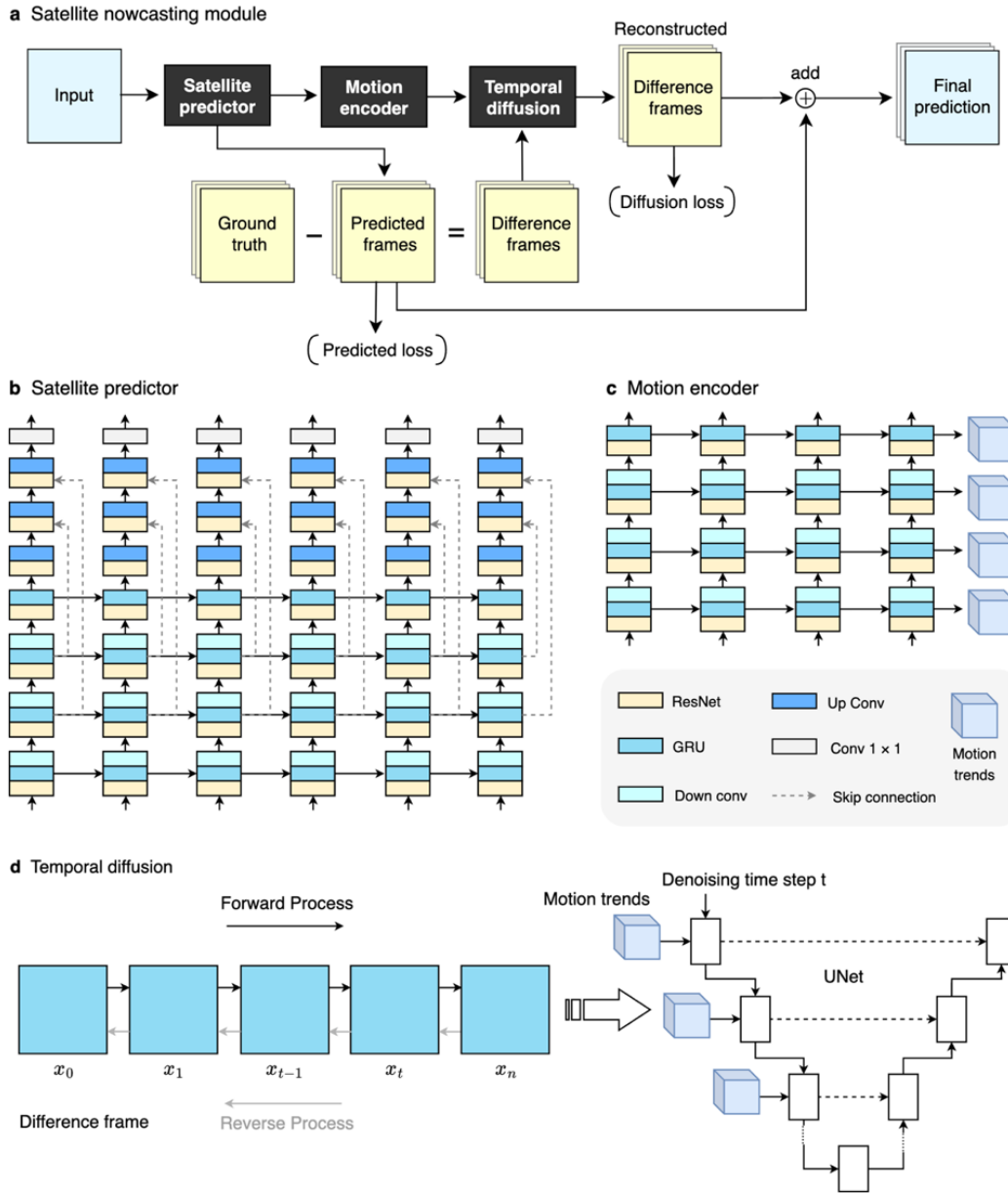
Additional information

Supplementary information

Supplementary Information is available for this paper.

Correspondence and requests for materials

Correspondence and requests for materials should be addressed to lixutao@hit.edu.cn.



Extended Data Fig. 1: Pipelines of the satellite nowcasting module. **a**, The overall layout of the satellite nowcasting module, which contains a satellite predictor, a motion encoder, and a temporal diffusion part. The satellite predictor accounts for producing the predicted sequence with given historical frames. With the guidance of the motion encoder, the temporal diffusion part aims to model temporal evolution dynamics of difference sequences between the prediction and observation. The final prediction is obtained by combining the predicted sequence and the reconstructed difference sequence. **b**, The architecture details of the satellite predictor, which contains multiscale GRU units. **c**, The architecture details of the motion encoder, which is an encoder part of the satellite predictor and has independent parameters. **d**, The workflow of the temporal diffusion part for i -th difference satellite frame. The conditional UNet is employed to predict a noise in the reverse process.